LAWRENCE
LIVERMORE
NATIONAL
LABORATORY

LLNL-CONF-425235

Underwater Blast Experiments and Modeling for Shock Mitigation

L. Glascoe, L. McMichael, K. Vandersall, J. Margraf

March 8, 2010

14th International Detonation Symposium
Coeur D'alene, ID, United States
April 11, 2010 through April 16, 2010

Disclaimer

Underwater Blast Experiments and Modeling for Shock Mitigation

Lee Glascoe, Larry McMichael, Kevin S. Vandersall and Jon Margraf

Lawrence Livermore National Laboratory, Livermore, California USA

Abstract. A simple but novel mitigation concept to enforce standoff distance and reduce shock loading on a vertical, partially-submerged structure is evaluated using scaled aquarium experiments and numerical modeling. Scaled, water tamped explosive experiments were performed using three gallon aquariums. The effectiveness of different mitigation configurations, including air-filled media and an air gap, is assessed relative to an unmitigated detonation using the same charge weight and standoff distance. Experiments using an air-filled media mitigation concept were found to effectively dampen the explosive response of the aluminum plate and reduce the final displacement at plate center by approximately half. The finite element model used for the initial experimental design compares very well to the experimental DIC results both spatially and temporally. Details of the experiment and finite element aquarium models are described including the boundary conditions, Eulerian and Lagrangian techniques, detonation models, experimental design and test diagnostics.

Introduction

Underwater explosions are efficient at the propagation of energy. Coupling the relatively high density with the incompressibility of water makes for enhanced shock transmission when compared to an air-blast of the same threat size (Cole, 1948). For enclosed air-filled structures or ship hulls below the waterline, damage associated with shocks from a nearby underwater blast can be much more severe than damage associated with an air-blast from a similar sized threat.

Effective mitigation of vulnerable structures against underwater shock is often best achieved by forcing increased standoff distance from the structure and by redistributing and/or breaking up the incident shock using air-filled material to maximize the impedance mismatch between materials, a function of density and sound speed. It is towards this end that we investigate the relative performance of a proposed mitigation option for a large concrete and steel structure: a belt of air-filled tubes encasing the waterside of an enclosed structure.

A series of small (3-gallon) aquarium tests described here evaluates the response of an underwater explosion with and without mitigation near the charge. These studies were then followed by a set of 70-gallon aquarium studies to be discussed in a follow-on paper. The aquarium experiments have been coupled closely with numerical simulation for pre-test prediction and post-test comparison. The primary goal of the study is to couple the experimental results to numerical simulation for code validation and to build confidence in the proposed mitigation scheme. The secondary goal is to build a test-bed for narrowing down diagnostics to be used in the

larger 70-gallon aquarium follow-on tests. The ALE3D hydrodynamics code was used for experiment design, pre-experiment deformation predictions, and post-experiment sensitivity studies.

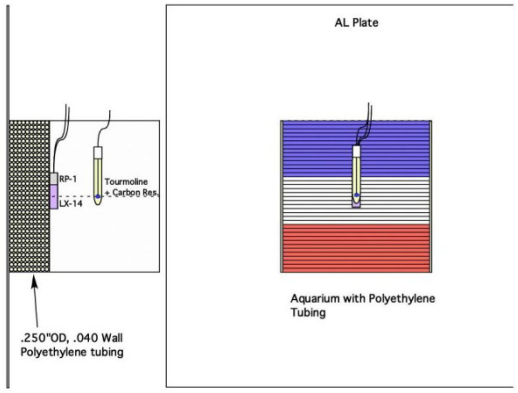

Fig. 1. Profile (left) and water-side (right) design drawings showing the aluminum plate, tourmaline pressure gauge, carbon resistor transducers, LX-14 explosive charge, RP-1 detonator, and proposed mitigation. The strain gauges that were bonded to the aluminum plate are not evident in the figure.

Experiment Design

Several scaled 3-gallon aquarium experiments were designed including water-tamped tests without mitigation, water-tamped tests with mitigation, and an air-blast (control) test. A non-rupturing scenario was chosen for ease of model validation.

The charge depth was chosen such that the failure of the sides of the aquarium and the free surface would not affect the short-term aluminum plate structural response associated with the primary shock event. Because the aquarium shatters immediately after the initial shock, this study does not include any relatively longer timescale analysis of bubble formation or collapse.

The charge weight and standoff distance for the experiments were selected to induce significant plastic strain in the aluminum plate, without rupturing it, for the unmitigated case based upon ALE3D analysis. For direct comparison of the effect of the mitigation only, i.e., discounting the effect of standoff, the 'unmitigated' test had the charge placed a standoff distance equal to the thickness of the overall mitigation scheme.

The 3-gallon aquariums used for the water-tamped study were nominally cubes with 24 cm (9.5 inches) on a side made from 6.35 mm (1/4 inch) Lucite. Explosive charges were 6.3 grams of LX-14 (95% HMX and 5% Estane by weight) initiated by an RP-1 detonator. One side of the aquarium was replaced with a 3.2 mm (1/8 inch) thick 6061-T6 aluminum plate, allowing the plate dimensions to extend well beyond the aquarium. This reduces the boundary effects introduced from holding the plate to a unistrut frame. For the mitigation, air-filled polyethylene mitigation tubes with 1.02 mm (0.040 inch) wall thickness and 6.35 mm (1/4 inch) nominal outside diameter were horizontally aligned in a regular pattern. Standoff distance from plate to surface of explosive was 6.35 cm (2.5 inches) for all cases (see Fig. 1).

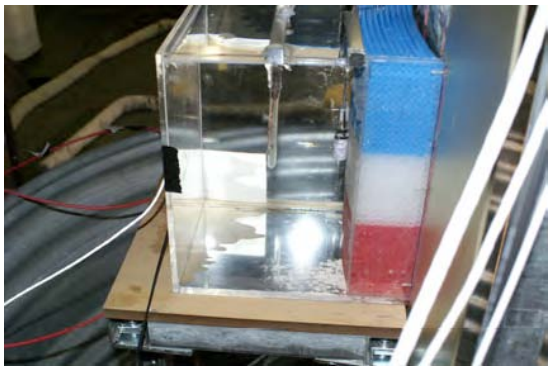

Fig. 2. Experimental set-up of one of the 3-gallon mitigation aquarium tests.

Fig. 3. Aluminum plate with illuminated speckle pattern for the DIC system and two of the 1000-Watt lights for illumination.

Several diagnostics were utilized in this test series including carbon resistor piezoresistive pressure gauges (e.g., Garcia et al., 2001), tourmaline piezoelectric pressure gauges, strain gauges, photonic doppler velocimetry (Strand et al., 2006), and digital image correlation (DIC) (Sutton et al., 2009; Nansteel and Chen, 2009) for measuring the displacement field on the plate exterior with corresponding 1000-Watt lighting and high-speed Phantom digital cameras (see Fig. 2 and 3). The aluminum plates were also physically measured after each test.

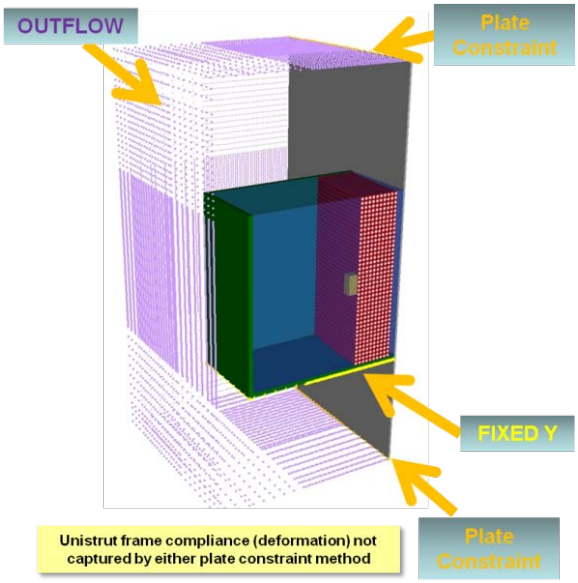

Fig. 4. Highlights of the ALE3D finite element model built for this study. Shown are material and boundary highlights for the water-tamped mitigation study.

Numerical Model

Detonation, shock transmission and structural response were numerically simulated using the ALE3D hydrocode (Nichols, 2008), an arbitrary-Lagrange-Eulerian (ALE) finite element code which predicts fluid-structure interaction and elastic-plastic material response on an unstructured grid and has the ability to model fully-coupled blast and structural interactions (Zukas, 2004). The major components of the code utilized for this study were explicit and implicit continuum-mechanics based rate formulations for mass, momentum and energy balance (see Eq. 1). All modeled components participate in advection and operate with slide surfaces.

$$\frac{\partial \rho}{\partial t} = -\frac{(\partial \rho u_i)}{\partial x_i} \qquad \rho \frac{Du_j}{Dt} = \frac{\partial}{\partial x_i}(\sigma_{ij}) \qquad \rho \frac{DE_T}{Dt} = \frac{\partial}{\partial x_i}(\sigma_{ij} u_j) \tag{1}$$

A finite element model of the mitigated water-tamped experiment is illustrated in Fig. 4. After initial mesh resolution study, a predictive model of 280,000 elements was created to capture resolution down to 2.5 mm (in and near the charge). Plate elements are modeled Lagrange while all others are modeled ALE. The six materials are highlighted as Al-6061 in gray, LX-14 in yellow, water in blue, Lucite in green, polyethylene in red, and air in white. The aluminum was represented by a Johnson-Cook material model using typical material properties; Lucite and polyethylene were modeled using standard elastic-plastic failure models; air was defined using a Gamma Law gas equation of state (EOS) at 20^{o}C and 1 bar atmosphere; a Gruneisen EOS was used for water; and LX-14 was modeled using a Jones-Wilkins-Lee (JWL) EOS assuming instantaneous volume burn (Dobratz, 1981).

The following boundary conditions are illustrated in Fig. 4: a vertical symmetry plane exists through the charge center and normal to the plate thickness, the plate is constrained on its top and bottom edges (orange), and outflow boundaries are enforced elsewhere (purple). Simulations using this model took approximately 60 hours on 16 processors to simulate 15 milliseconds after detonation initiation.

Initial predictive ALE3D simulations assumed a clamped boundary condition (boundary condition 1 or “BC1”), prohibiting all movement for the upper and lower one-inch sections of the aluminum plate through the thickness. The influence that the numerical boundary conditions have on the aluminum plate’s response was investigated by replacing the original clamped boundary condition with a pinned condition, fixing a single line of nodes across the top and bottom edges of the plate (boundary condition 2 or “BC2”).

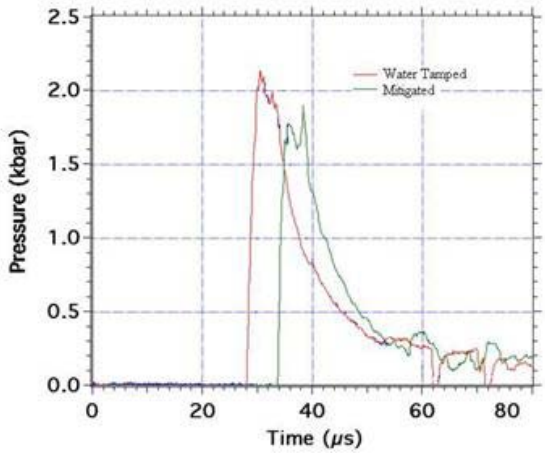

Fig. 5. Experimental tourmaline pressure gauge output for water tamped (red line) and mitigated tests (green line).

Results and Discussion

Empirical Results

According to Cole's correlations for free-field underwater TNT explosions, the peak shock wave pressure (in psi) and integrated impulse per unit area (in psi-seconds) can be estimated by:

$$P_m = 2.16 \times 10^4 \, (W^{1/3}/R)^{1.13} \qquad (2)$$

$$I/A = 1.46 \, W^{0.63}/R^{0.89} \qquad (3)$$

W is in lb-f and R in ft. The results P_m and I/M are calculated as psi and psi-sec, respectively. For this 6.3 grams of LX-14 (1.32 TNT equivalency), the peak shock pressure at 2.5 inches is 1.9 kbar (28000 psi) and an impulse of ~30 kbar-μsec (0.5 psi-seconds) which corresponds well with recorded results of the unmitigated blast at the tourmaline gauge (Fig. 5, red line) where 2.2 kbar was recorded in peak pressure. The slightly lower peak pressure and impulse recorded by the tourmaline gauge in the presence of mitigation (Fig. 5, green line) is likely due to decreased charge tamping, i.e., the charge was in contact with the plastic tubes and was therefore not completely water-tamped.

For the water-tamped tests, the combination of DIC and post-test deformation measurements allow the numerical and experimental results to be compared for both the plate's transient response to the shock wave and the plate's final (residual) deformation. Final deflection of the aluminum plates was visibly more for the unmitigated water tamped case (Fig. 6) than for the mitigated case (Fig. 7). This deflection was physically measured at discrete locations after each test and compared to ALE3D predictions. Comparisons at the plate center are illustrated in Fig. 8 for unmitigated and Fig. 9 for mitigated tests. Post-test plate deformations were noted when the clamping fixtures were removed for final deflection measurements, indicating the presence of stored energy in boundary compliance, particularly in the unmitigated experiment. ALE3D simulations were then reexamined using the pinned BC2 boundaries for the aluminum plate. Table 1 lists the final deformation measured for each plate in the center of the plate and the modeled late time (after ~8 milliseconds) deformation for the two boundary conditions.

Numerical Results

Both empirical and numerical results show that mitigation reduces final deflection by about half. The mitigated model prediction of final deflection (Table 1) using BC1 and BC2 bracket the empirical deformation while the unmitigated models with BC1 and BC2 both under-predict deformation, with the latter being very close to test deflection. Such differences may reflect the relative importance of the plate boundary and the unistrut frame compliance on model results for larger impulses, i.e., the unmitigated scenario (Fig. 8), since the time evolving response of the BC2 boundary seems more appropriate than the initial BC1 modeled conditions for unmitigated conditions. In the mitigated case, the mounting at the plate boundary is of secondary importance, with the two representations of the boundary neatly containing the response of the actual structure (Fig. 9).

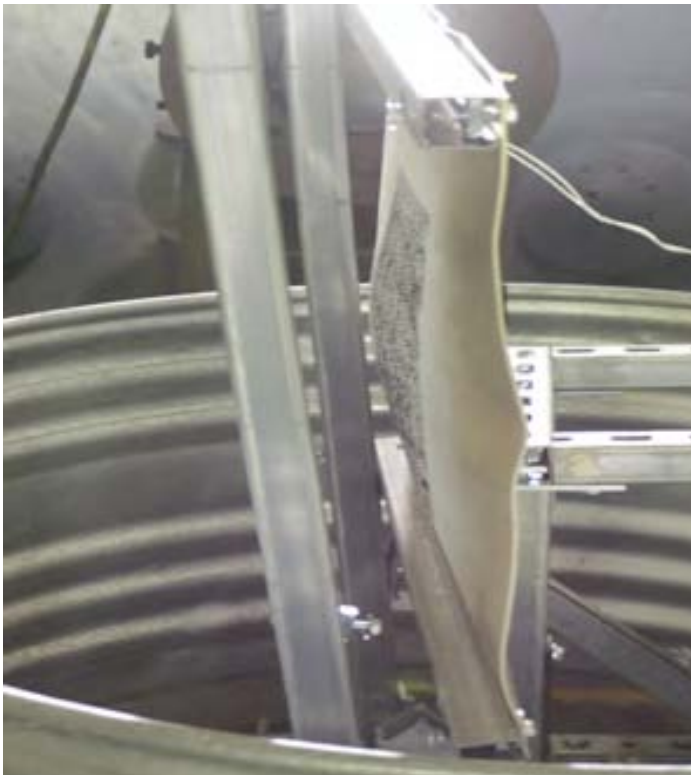

Fig. 6. Post-test, unmitigated, water-tamped plate deflection; note that aquarium is no longer present.

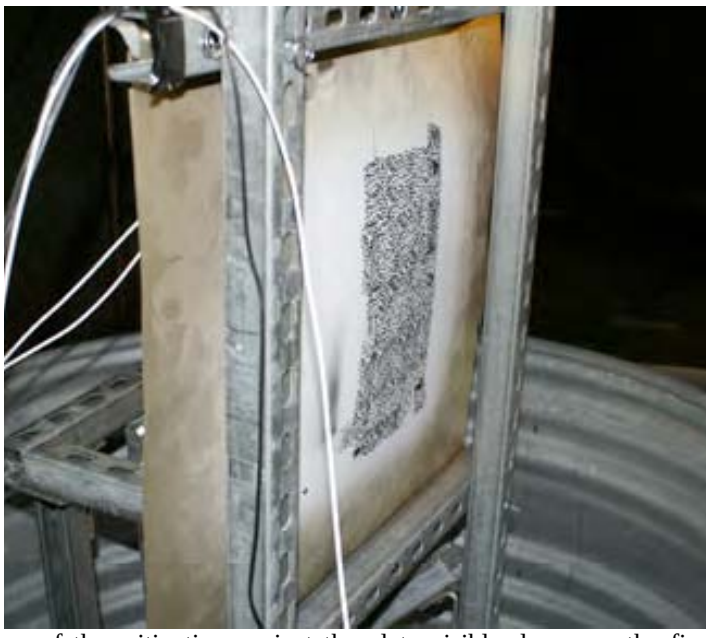

Fig. 7. The presence of the mitigation against the plate visibly decreases the final deflection shown above.

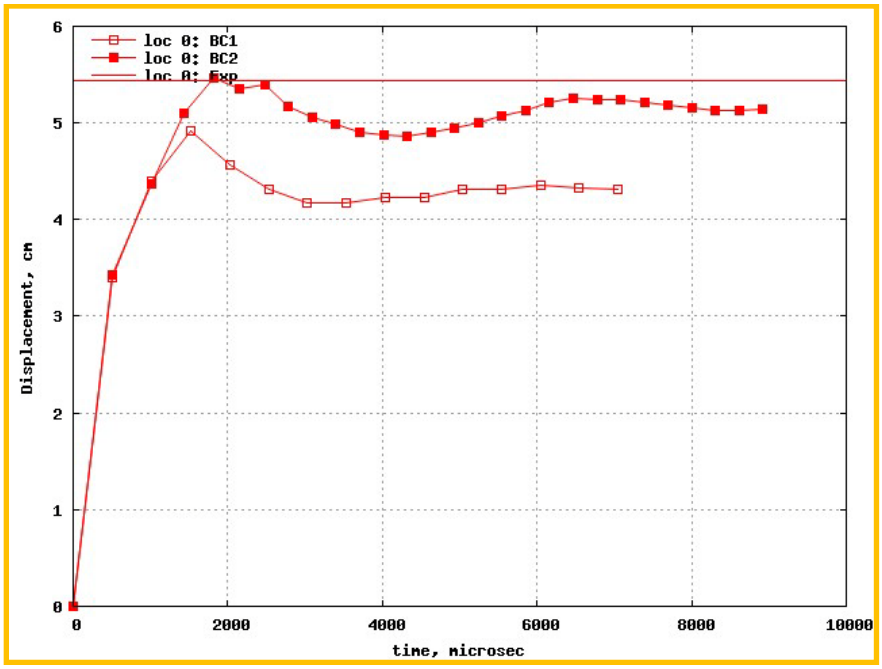

Fig. 8. Measured center point displacement for the unmitigated test (solid straight line at 5.4 cm) and numerically predicted time history results (open points for BC1 and filled points for BC2).

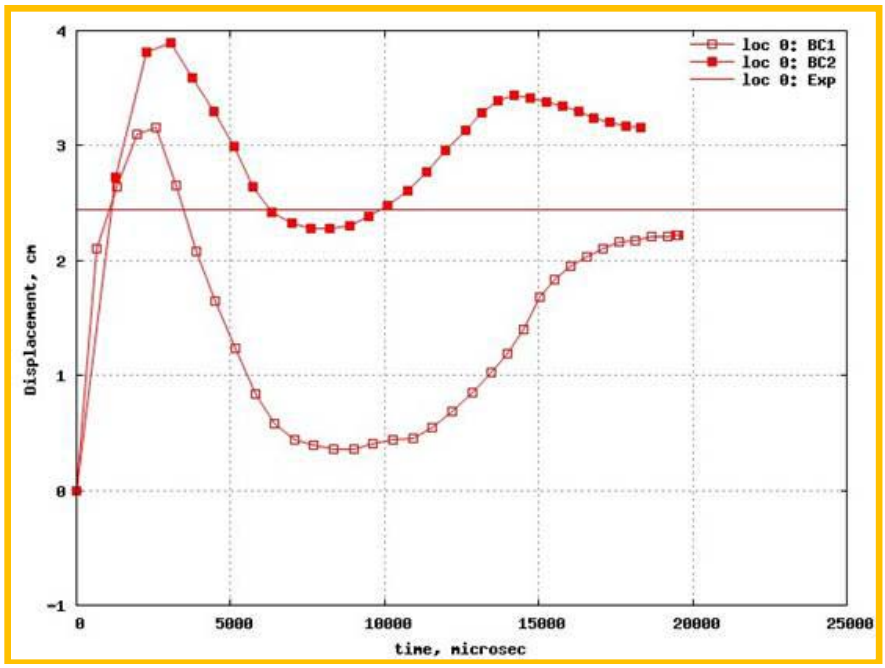

Fig. 9. Measured center point displacement for the mitigated test (solid straight line at 2.4 cm) and numerically predicted time history results (open points for BC1 and filled points for BC2).

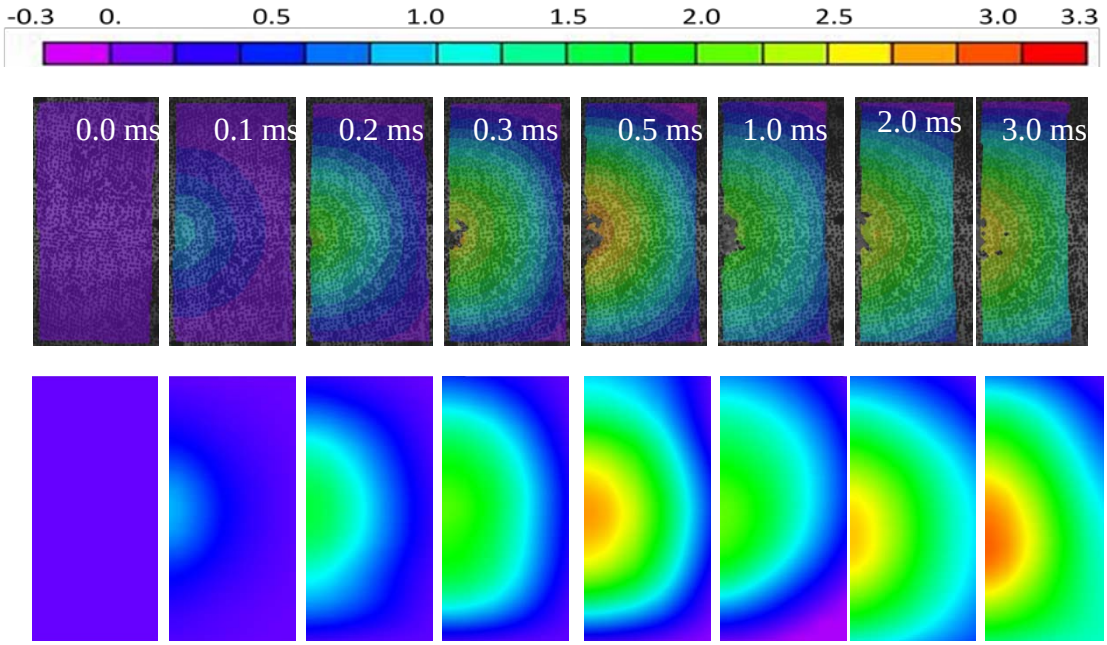

Fig. 10. Half-symmetry Digital Image Correlation (DIC) experimental measurements in centimeters (see color bar) of relative plate deflection (top images) compare well with ALE3D simulation of plate deflection (lower images) for the unmitigated test over the first three milliseconds.

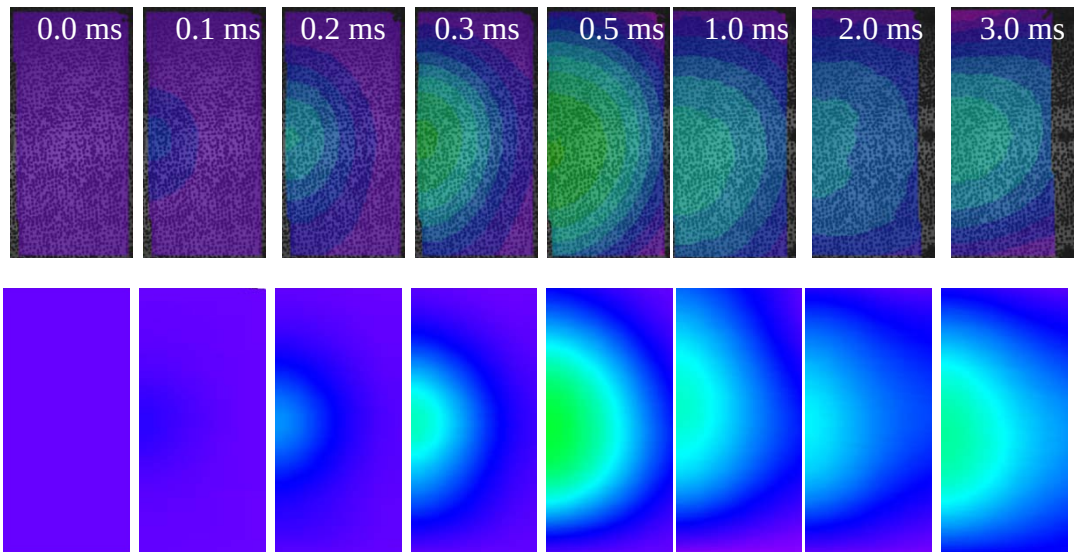

Fig. 11. Half-symmetry DIC plate deflection measurements (top images) in centimeters (same color bar) compare well with ALE3D simulation of plate deflection (lower images) for the mitigated test over the first three milliseconds.

Table 1. Experimental ("test") and modeled deflection at center of aluminum plate (in centimeters) for two different modeled boundary conditions on the plate ("BC1" and "BC2") at late time.

3-gallon Scenario	test	Model BC1	Model BC2
Unitigated	5.4	4.3	5.2
Mitigated	2.4	2.2	3.2

The temporal and full spatial field response of the aluminum plate's *relative* displacement is captured by the DIC measurements and compares well with numerical predictions for both BC1 (not shown) and BC2. The relative displacement is the displacement of the plate relative to the upper right-hand corner of the image. Fig. 10 and Fig. 11 illustrate this relative response in the half-symmetry of the plate (only half of the aluminum plate was speckled for DIC for the 3-gallon tests). The temporal agreement between model and experiment is illustrated in both cases with a peak in response occurring at around 0.5 milliseconds and again at 3.0 milliseconds. Note how the model captures the empirical timing of structural ringing between 0.5 and 3.0 milliseconds. Also of note is the spallation spots (black regions) on the DIC images of the unmitigated response near the center of Fig. 11 after 0.3 milliseconds; at this point, part of the paint used to form the speckle pattern for image correllation on the aluminum was spalling off due to the shock.

Conclusions

The unmitigated case provides a baseline response for the temporal and spatial deformation in the aluminum plate for comparison to the mitigated case. This establishes a relative effectiveness metric to evaluate the proposed air-filled media mitigation method. Experiments confirmed that the mitigation concept effectively dampens the explosive response of the aluminum plate, reducing the final displacement at plate center by approximately 50%. The unmitigated, water-tamped experiments compare well with the numerical predictions, particularly when accounting for the effects of boundary conditions on the aluminum plate.

These experimental results help validate a numerical approach for evaluating structural response to an underwater explosive shock at different scales. Further, the consistent and significant reduction in deflection of the aluminum plate in the presence of the proposed mitigation option builds confidence in the ability of such schemes to provide protection against large explosive shocks for full-scale structures. Follow-on work with a larger 70-gallon aquarium tank impulse-scaled from these 3-gallon studies, will further build confidence in the mitigation approach and provide further validation of the use of an arbitrary-Lagrange-Eulerian (ALE) model for the prediction of structural response to mitigated and unmitigated underwater explosive blasts.

Acknowledgements

Special thanks go to Frank Garcia, Daniel Greenwood, Franco Gagliardi, Bruce Cunningham, Gregory Silva and Noel Tan for their guidance with the testing at the High Explosives Application Facility (HEAF) at LLNL. We would also like to acknowledge the assistance of Dr Charles Noble and Dr Jon Maienschein for their review of experimental design and Mr Christopher McKay and Dr. John Fortune for their support of this study. This work performed under the auspices of the U.S. Department of Energy by Lawrence Livermore National Laboratory under Contract DE-AC52-07NA27344. This is LLNL-CONF-425235. This work is sponsored by the Department of Homeland Security Science and Technology Directorate's Infrastructure and Geophysical Division.

References

Cole, H. Underwater Explosions, Princeton University Press, Princeton, NJ, (1948).

Dobratz, B. M. "LLNL Explosives Handbook, Properties of Chemical Explosives and Explosive

Simulants," UCRL-52997, Lawrence Livermore National Laboratory, 1981.

Garcia, F., Forbes, J.W., Tarver, C.M., Paul A. Urtiew, P.A., Greenwood, D.W., and Vandersall, K. "Pressure Wave Measurements from Thermal Cook-off of an HMX Based High Explosive PBX 9501," 12th APS Conference on Shock Compression of Condensed Matter, Atlanta, GA, June 245-29, (2001).

Nansteel, M.W. and Chen, C.C. "High-Speed Photography and Digital Image Correlation for the Study of Blast Structure Response," ITEA Journal, 30, pp. 45-56, March 2009.

Nichols III, A. L., ed. (2008). "Users Manual for ALE3D, An Arbitrary Lagrange/Eulerian 2D and 3D Code System." Volumes 1 and 2, UCRL-MA-152204 Rev. 7, Lawrence Livermore National Laboratory.

Strand, O. T, D. R Goosman, C. Martinez, T. L. Whitworth, and W. W. Kuhlow, "A Novel System for High-Speed Velocimetry Using Heterodyne Techniques," Rev. Sci. Instrum., 77, 083108, 2006.

Sutton, M.A., J. Orteu, and H.W. Schreier, "Image Correlation for Shape, Motion, and Deformation Measurements: Basic Concepts, Theory, and Applications," Springer Press, 2009.

Zukas, J. Introduction to Hydrocodes, Studies in Applied Mechanics, 49. Elsevier, New York, 2004.